Virtual aggregate interlock testing using real crack surfaces from 3D scanning

Lu, Jiandong; Hendriks, Max A.N.; Walraven, Joost; Yang, Yuguang

DOI
10.1016/j.engstruct.2025.120963

Publication date
2025

Document Version
Final published version

Published in
Engineering Structures

Engineering Structures 343 (2025) 120963

Contents lists available at ScienceDirect

Engineering Structures

journal homepage: www.elsevier.com/locate/engstruct

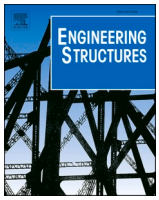

Virtual aggregate interlock testing using real crack surfaces from 3D scanning

Jiandong Lu [a,*], Max A.N. Hendriks [a,b], Joost Walraven [a], Yuguang Yang [a]

[a] Deparment of Engineering Structures, Delft University of Technology, Stevinweg 1, Delft 2628CN, the Netherlands
[b] Department of Structural Engineering, Norwegian University of Science and Technology, Richard Birkelands vei 1A, Trondheim 7491, Norway

ARTICLE INFO

Keywords:
Aggregate interlock
Surface roughness
3D scanning
Shear resistance
Crack surface

ABSTRACT

Aggregate interlock is considered one of the most important shear transfer mechanisms in concrete members. In the well-established Two-Phase model proposed by Walraven in the 1980s, the shear stress transferred by aggregate interlock is estimated by calculating the projected contact areas of two crack surfaces. As one of the main assumptions in the model, the crack surface is idealized by a plain surface crossing randomly distributed, idealized spherical aggregates. This was a necessary simplification of an actual crack surface in the 1980s because of the lack of measurement equipment as well as computational capacity. With the development of high-accuracy 3D scanning techniques, new possibilities for modelling aggregate interlock have become available. This paper proposes a generalised method to determine the aggregate interlock stresses using the crack surface directly from 3D scanning. The proposed method is cross-verified with the Two-Phase model using the same simplified crack surfaces. A case study using the scanned crack surfaces of concrete cubes is conducted to investigate the influence of surface roughness. The proposed method provides a new possibility for conducting a refined investigation of the aggregate interlock for new concrete types, especially under the scope of the next-generation Eurocode shear provision.

1. Introduction

Shear stress can be transferred across a crack in concrete when the crack opening is relatively small. This phenomenon is commonly known as aggregate interlock. Aggregate interlock is considered one of the most important shear transfer mechanisms in cracked reinforced concrete (RC) members. Between the 1960s and 1980s, several researchers conducted detailed investigations into this topic, and several mechanical models were developed, such as the Two-Phase Model proposed by Walraven [1], the Contact Density Model proposed by Li et al. [2,3] and the Rough Crack Model proposed by Bazant and Gambarova [4]. Among those models, the Two-Phase Model has a wide application in the design practices of concrete structures. It is adopted and recognized by many theoretical models for the shear behaviour of RC members, such as the Modified Compressive Field Theory [5], the Critical Shear Crack Theory [6,7], the Critical Shear Displacement Theory [8,9], the Shear Crack Propagation Theory [10], and the Compression Chord Capacity Model [11–13]. These models eventually lead to the modern design code provisions for shear such as the Model Code [14], and the next-generation Eurocode [15]. Within this scope, it is needed to have an objective way to determine the aggregate interlock stresses for different types of concrete. This paper proposes a computer-aided method to determine the aggregate interlock stresses within the theoretical framework of the Two-Phase model.

Although the Two-Phase model has been widely applied, it was derived and calibrated in the 1980s, focusing on the 'regular' concrete at that time. In the past 40 years, one has witnessed a leap in concrete technology. More recent types of concrete such as lightweight aggregate concrete (LWA), and high-strength concrete have been applied in engineering practices. As many researchers pointed out [16–18], smoother crack surfaces are observed in high-strength concrete and LWA concrete because of the fracture of aggregates. In those cases, lower aggregate interlock stresses are expected. When the Two-Phase model is used for a concrete type where aggregate cracking can be expected, the way to deal with that up to now has been quite simple, by just introducing a reduction factor between 0 and 1 for the contact area (e.g. 0.35 in Model Code [19]). Some other empirical reduction factors can be found in [17,20,21]. Although introducing a reduction factor is valid for some cases, it could be too simple for other cases, especially for types of concrete where most or partial aggregates are expected to be cracked.

* Corresponding author.
E-mail address: J.Lu-1@tudelft.nl (J. Lu).

https://doi.org/10.1016/j.engstruct.2025.120963
Received 19 January 2025; Received in revised form 13 June 2025; Accepted 12 July 2025

Some numerical studies have employed mesoscopic numerical approaches, including both continuum-based (e.g., FEM) [22–24] and discrete element methods (DEM) [25,26], to investigate how aggregates affect the mechanical properties and fracture process of concrete. These models simulate the interaction of aggregates and matrix material at the meso-scale, capturing crack propagation and stress transfer mechanisms. While these approaches provide valuable insights into the micromechanical behaviour, they mainly focus on the influence of aggregates on the concrete compressive and tensile behaviour.

Therefore, a more general and systematic way to quantify the influence of surface roughness on aggregate interlock contribution within the scope of the physical-based aggregate interlock model is still needed. This is especially necessary with the introduction of the next-generation Eurocode shear provision [15] in which the size parameter d_{dg} is linked to the aggregate size.

To do this, one of the main challenges is to describe a realistic crack surface of the new concrete type as what has been done in the Two-Phase model. Such a model typically requires a detailed analysis of cracking features, the distribution of aggregates in new types of concrete, and a large amount of test data for the model validation. Such resources are not always available. As an alternative approach, one can obtain the crack surfaces much easier nowadays with the development of high-accuracy 3D scanners [21]. In engineering practices, splitting tensile tests are often applied to evaluate the tensile strength of a concrete. In such tests, a localized crack surface is generated under tension. This is similar to a typical shear crack of an RC member. If the contribution of aggregate interlock can be determined based on those crack surfaces generated in splitting tensile tests, it is then an attractive option for engineers when they design the shear resistance of a structural member with new types of concrete. A similar approach has been suggested by Presvyri and Yang et al. in [27]. Their investigation was conducted in a 2D manner. The aggregate interlock contribution determined by this method highly depends on the analysed cross-section, which can bring high uncertainties.

This paper proposes a generalised method to determine the normal and shear stresses generated by aggregate interlock by an actual crack surface based on 3D scanning. The proposed method can consider the irregularity of an actual crack surface and is verified using a simulated surface based on the same assumptions used in the Two-Phase model. Then, the aggregate interlock contribution obtained from the actual crack surface using the proposed method is presented and discussed. The results are also compared to theoretical predictions from several existing analytical aggregate interlocking models. The proposed method provides new possibilities for further investigation of the influence of surface roughness and kinematic conditions on aggregate interlock stresses.

2. Brief overview of the Two-Phase Model

The main concepts of the Two-Phase model are depicted in Fig. 1. The model describes a crack surface in concrete by a plane crossing the surfaces of aggregates embedded in the concrete paste. The distance between the centre of the aggregate and the cracked plane is defined as

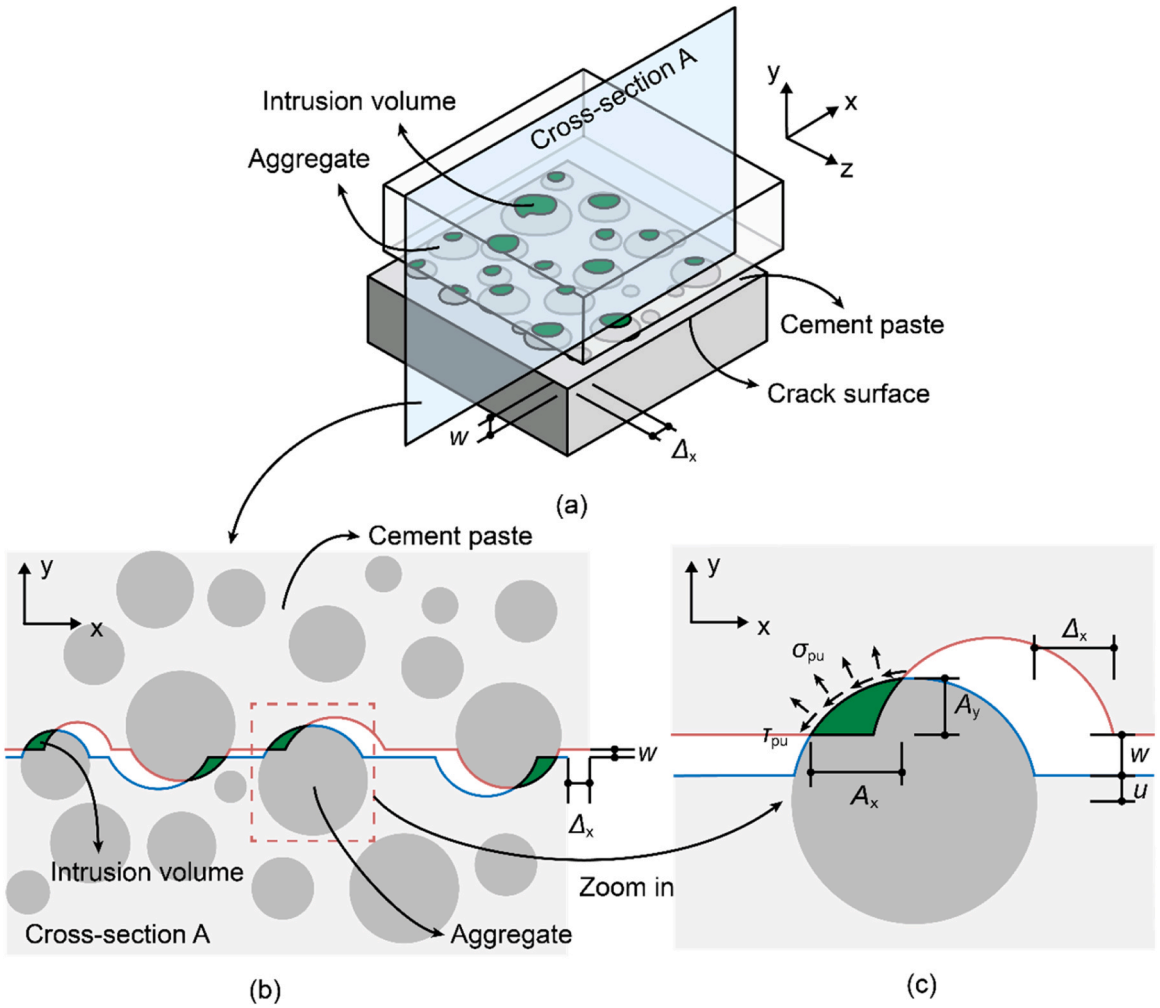

Fig. 1. Schematic illustration of the Two-Phase model adapted from [1]: (a) intrusion volume due to sliding; (b) intrusion volume between the cement paste and aggregates in cross-section A; (c) contact stresses on a single aggregate.

the embedded depth u. It further assumes that the aggregates are perfect spheres and follow Fuller's distribution curve [28]. The cement paste is assumed to be a rigid-plastic material with yielding strength σ_{pu}, without consideration of yield condition and normality to the yield surface. Thus, shear and normal stresses arise when the aggregates intrude on the yielding cement paste under a given displacement between crack surfaces. The magnitudes of the stresses are related to the projected area in the x and y direction of the intrusion volume of the aggregates, namely A_x and A_y, as indicated in Fig. 1c. The detailed derivation of the model can be found in [1]. The model shows good accuracy compared to experimental data obtained from push-off tests, especially for the concrete with cube compressive strength lower than 60 MPa [1,29].

3. Methodology

3.1. Overview

As explained, to account for the surface roughness of a random concrete mixture more accurately, we propose to use directly the 3D scanned measurement instead of the simplified crack surface suggested in the Two-Phase model. By applying displacement to the crack surface, the intrusion volume can be obtained and used to determine A_x and A_y in the Two-Phase model. Here, we assume that the aggregate interlock stresses along the crack can still be described by A_x and A_y according to the Two-Phase model:

$$\begin{bmatrix}\sigma\\ \tau\end{bmatrix} = \sigma_{pu}\begin{bmatrix}1 & -\mu\\ \mu & 1\end{bmatrix}\begin{bmatrix}A_x\\ A_y\end{bmatrix} \tag{1}$$

$$\sigma_{pu} = 6.39 \times \left(f_{c,cube}\right)^{0.56} \text{ in MPa} \tag{2}$$

in which σ_{pu} is the yielding strength of the cement paste. Because the cement paste is assumed to be a rigid-plastic material, σ_{pu} becomes the contact pressure between the concrete paste and aggregates, $\mu = 0.4$ is the friction coefficient and $f_{c,cube}$ is the cube compressive concrete strength.

Fig. 2 summarizes the main steps of obtaining the projected area proposed in this paper. The proposed method consists of five steps, namely acquisition of 3D scanning data, reconstruction of the crack surface, implementation of crack kinematics, determination of intrusion volumes and projected areas, and calculation of aggregate interlock stresses. The following sections present the concepts and steps of the proposed method in detail. The demonstration is conducted based on a crack surface from a splitting tensile test specimen as discussed in the introduction, but it is generally applicable to any type of crack surface.

3.2. Acquisition of 3D scanning data

The concrete specimen used in this paper for the demonstration is a concrete cube (150 mm × 150 mm × 150 mm) made of geopolymer concrete. More information about the material can be found in [30]. Fig. 3a shows the crack surface after the splitting tensile test. It can be seen that many aggregates are broken in the crack surface due to the use of recycled aggregates, which contradicts the assumptions used in the Two-Phase model. The influence of this contradiction will be further discussed in Section 5.4 when compared to the theoretical models. The point cloud data used in this paper is obtained using a HandyScan BLACK handheld scanner from Creaform [31], but the data acquisition can be done by other 3D scanners. The used scanner can provide a maximum resolution of 0.025 mm. Fig. 3b shows the scanned point cloud. In literature [18,32,33], it is recommended to use a spacing close to 0.25 mm. In this study, the spacing for scanned surfaces is around

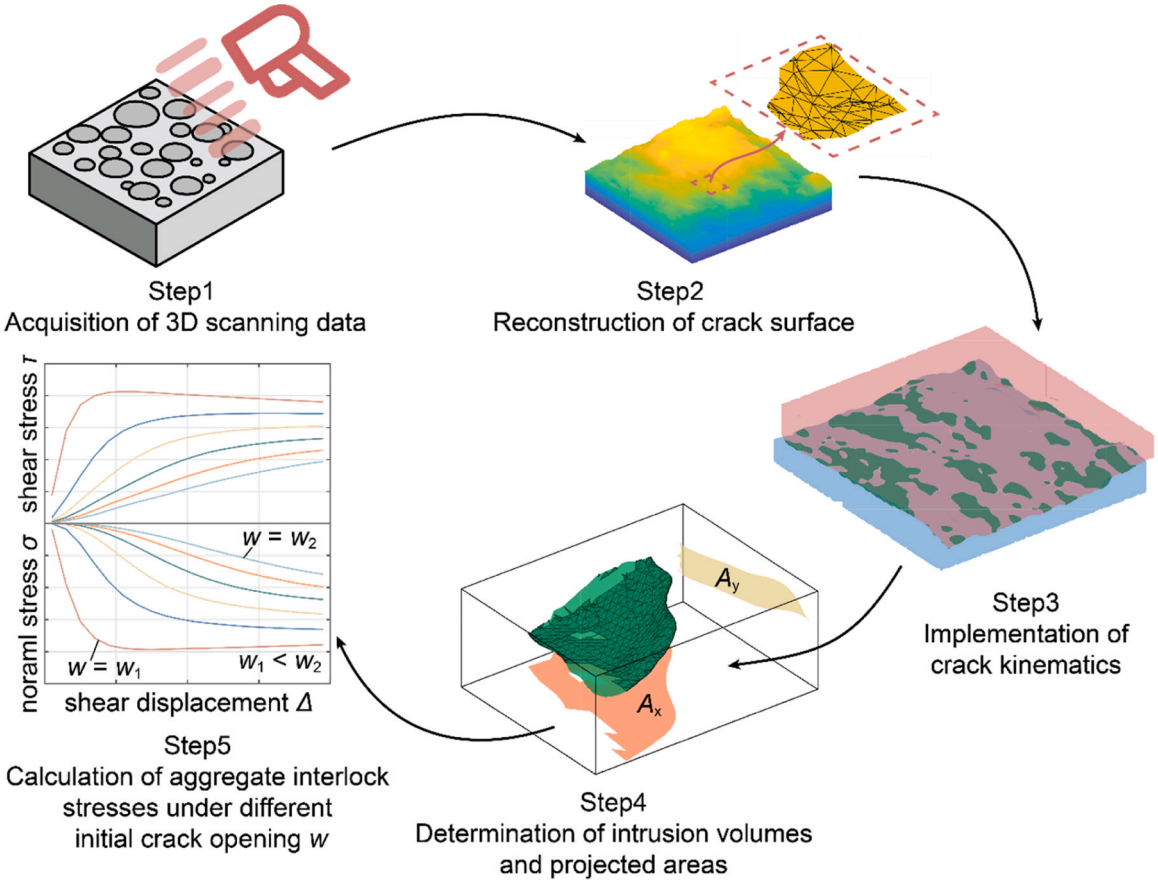

Fig. 2. Main steps and working flowchart of the proposed method.

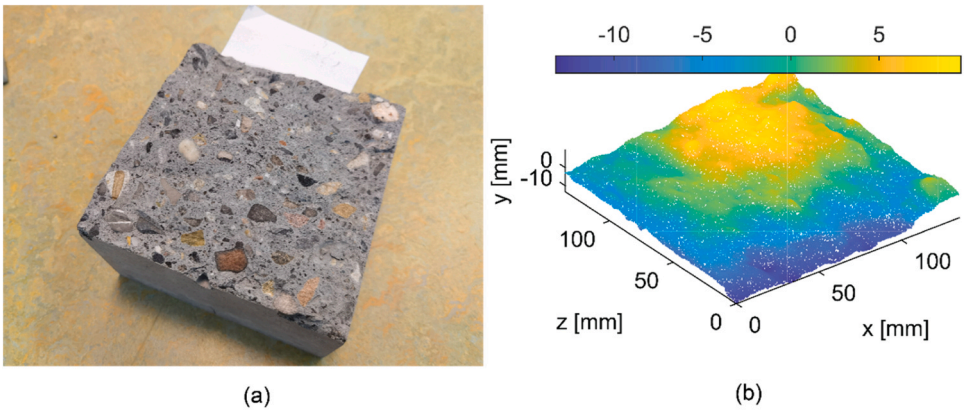

Fig. 3. The crack surface used for the demonstration: (a) crack surface after a splitting tensile test; (b) scanned point cloud of the crack surface.

0.20 mm.

3.3. Reconstruction of the crack surface

Once the scanned point cloud data is obtained, a 3D surface is reconstructed by the algorithm developed by Di Angelo et al. [34]. The algorithm allows a fast construction of 3D triangular meshes based on 3D point cloud data. Fig. 4a displays the meshes after the surface reconstruction and Fig. 4b illustrates how the points are connected. The same method can be applied to the reconstruction of the top surface. A total of 280,014 and 283,252 triangular meshes are generated for the bottom and top surfaces, respectively. A hidden assumption behind this step is that the geometrical irregularity of the crack surfaces from both sides of a crack is identical because we assume that the mismatched area between the two crack surfaces only consists of a small portion of the total crack surface. This assumption is also used in the Two-phase model. Although this assumption may not hold in reality, the main aim of this paper is to propose a general method to determine the aggregate interlock using 3D scanning. Fig. 4c depicts the final virtual specimen after assembling two surfaces.

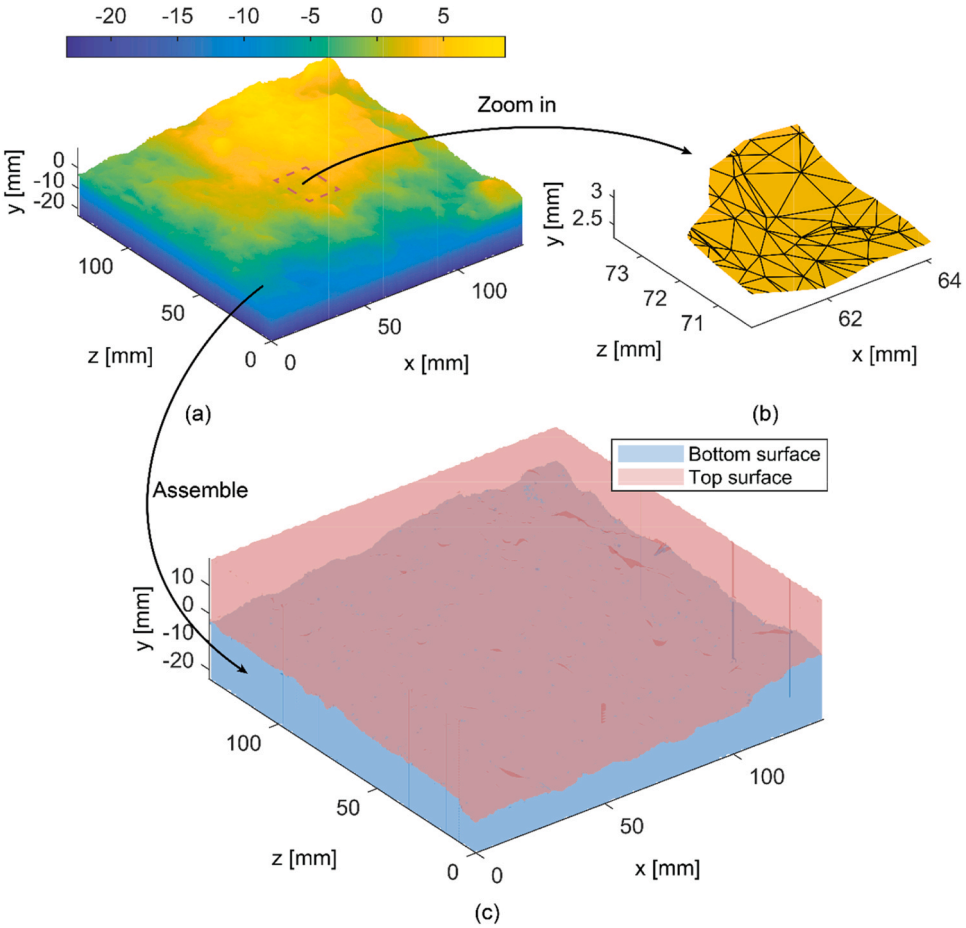

Fig. 4. Surface reconstruction from point cloud data: (a) triangular meshes after surface construction; (b) zoom-in view for triangular meshes; (c) virtual specimen after assembling two surfaces.

3.4. Implementation of crack kinematics

In general, a crack can experience two types of kinematics, namely opening w (Mode I) and sliding Δ (Mode II). These two kinematics correspond to the normal and tangential displacement along the crack surface, respectively. In the virtual test, the bottom surface is fixed and the crack kinematics are applied to the top surface. Then, the intrusion volume between two surfaces can be determined and used to calculate the projected areas.

In the following demonstration, the crack opening w is applied in the y-direction and the sliding Δ is applied in the x-direction. Since the bottom surface is fixed, these crack kinematics can be achieved by the following equation:

$$C_{\text{top,w,}\Delta} = C_{\text{top}} + T = \begin{bmatrix} x_{\text{top}} \\ z_{\text{top}} \\ y_{\text{top}} \end{bmatrix}' + \begin{bmatrix} \Delta_x \\ \Delta_z \\ w \end{bmatrix}' \tag{3}$$

where $C_{\text{top},w,\Delta}$ is the coordinates matrix of all vertices of the top surface after applying crack kinematics, C_{top} is the original coordinates matrix of all vertices of the top surface, and T is the global translation vector.

It should be mentioned that Eq. (3) is a generalized form to apply uniform crack kinematics. In the following analysis, only the sliding in the x-direction Δ_x is applied for the sake of simplicity. Fig. 5a shows the virtual specimen after implementing the crack kinematics.

3.5. Determination of intrusion volumes and projected areas

3.5.1. Boolean operation between two crack surfaces

After applying the kinematics to the virtual specimen, the top crack surface can partially intersect with the bottom surface and some intrusion volumes can be observed between the two closed surfaces. Essentially, these intrusion volumes are the volumes shared by the two closed surfaces. Therefore, the geometric conjunction (intersection) of the Boolean operation can be applied to the two closed surfaces to obtain intrusion volumes. We use the iso2mesh toolbox developed by Fang [35, 36] to achieve this goal. This operation is essentially a Boolean operation between two closed objects. After the Boolean operation, one of the intrusion volumes can be seen in Fig. 5b. With the intrusion volumes in hand, the projected areas can be further calculated.

3.5.2. Maximum contact phase in the Two-Phase model

In the Two-Phase model, a maximum contact phase is defined when the sliding Δ exceeds the maximum sliding value Δ_b. In this stage, the projected areas do not grow as the sliding increases. Part of the intrusion volume, highlighted by the dashed line in Fig. 6a, should be reduced in the calculation because of the fully plasticized mortar. To incorporate this phase in the proposed method, we use the outward unit normal vectors of the triangular meshes to select the meshes for calculating the projected area.

As shown in Fig. 6a, the outward unit normal vector is projected on the x-y plane first. Then, the angle α enclosed by the projected vector and the positive direction of the x-axis can be calculated. For sign convention, the clockwise direction from the projected vector to the positive direction of the x-axis is considered to be positive in this calculation. Then, by selecting the meshes with an angle α falling within the interval $(\pi/2, \pi)$ to calculate the projected areas, the maximum contact phase can be incorporated into the proposed method.

When it comes to the situation where the aggregate is embedded in the top crack surface, as shown in Fig. 6b. The bottom crack surface is fixed and the sliding is subjected to the top crack surface. In this situation, the meshes with an angle α falling within the interval $(3\pi/2, 2\pi)$ should be selected to calculate the projected areas.

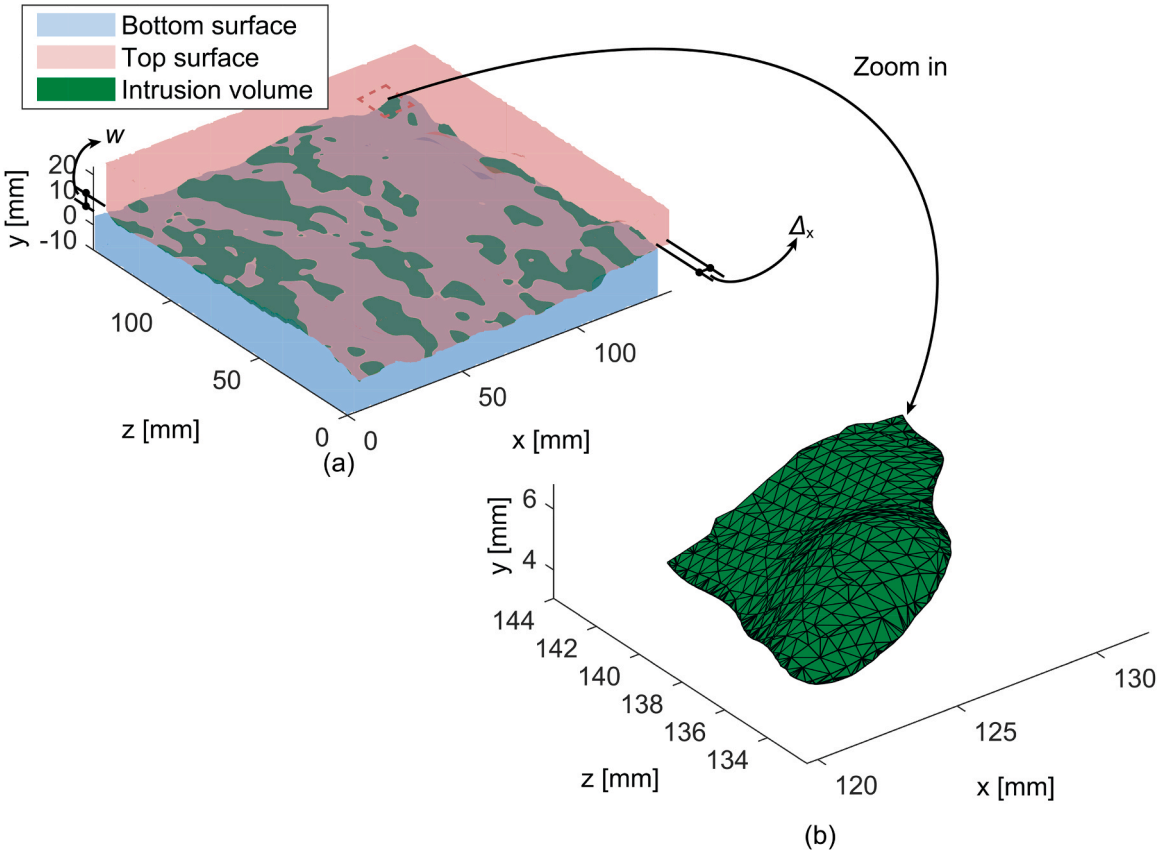

Fig. 5. Virtual specimen after applying crack kinematics ($w = 0.5$ mm, $\Delta_x = 5$ mm): (a) the overview of all intrusion volumes; (b) a zoom-in look at an individual intrusion volume.

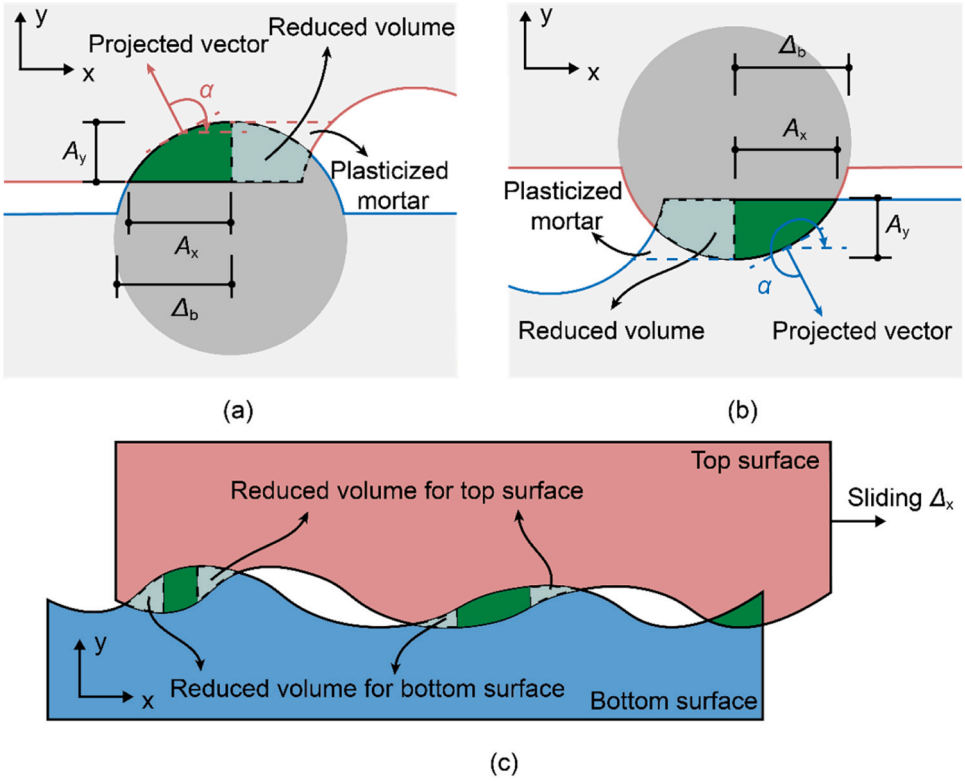

Fig. 6. Generalised maximum contact phase adapted from [1]: (a) case when the aggregate is embedded in the bottom surface; (b) case when the aggregate is embedded in the top surface; (c) case for two arbitrary crack surfaces.

The aforementioned selection criterion for meshes is established based on the fact that the crack surface where the aggregate is embedded is known. However, for a generally scanned crack surface, whether an arbitrary intrusion volume is an aggregate is unknown. Fig. 6c shows the intrusion volumes of two arbitrary crack surfaces. It can be seen that two different possible reduced volumes can be found. An additional step is needed to select the set of meshes to calculate the projected area.

3.5.3. *Selection of meshes for calculating the projected areas*

For a general intrusion volume, two groups of meshes can be selected based on the vector angle α. The meshes with an angle α falling within the interval $(\pi/2, \pi)$ are defined as the back meshes since the dot product between those projected vectors and the sliding direction is negative. For the meshes with an angle α falling within the interval $(3\pi/2, 2\pi)$, they are defined as the front meshes since the dot product between those projected vectors and the sliding direction is positive. With the two sets of selected meshes, the projected area of them can be calculated separately. The principle of the calculation of projected areas is illustrated in Fig. 7a. The projected areas A_x and A_y can be calculated using the following equations based on the selected meshes:

$$A_x = \sum_{i=1}^{N} a_i \cos(\mathbf{n}_i, \boldsymbol{e}_z) = \sum_{i=1}^{N} a_i \left| \frac{\mathbf{n}_i \cdot \boldsymbol{e}_z}{\|\mathbf{n}_i\| \|\boldsymbol{e}_z\|} \right| \tag{4}$$

$$A_y = \sum_{i=1}^{N} a_i \cos(\mathbf{n}_i, \boldsymbol{e}_x) = \sum_{i=1}^{N} a_i \left| \frac{\mathbf{n}_i \cdot \boldsymbol{e}_x}{\|\mathbf{n}_i\| \|\boldsymbol{e}_x\|} \right| \tag{5}$$

where A_x is the total projected area in the x-z plane, A_y is the total projected area in the y-z plane, N is the total number of triangular meshes, a_i is the area of the i^{th} triangular mesh, $\mathbf{n}_i$ is the outward normal vector of the i^{th} triangular mesh, $\boldsymbol{e}_x$, $\boldsymbol{e}_y$ and $\boldsymbol{e}_z$ are the unit basis vector of the global coordinate system.

Fig. 7b and c show the projected areas based on the front and back meshes respectively. To satisfy the requirement of the maximum contact phase, the selected meshes should maximize the sum of the projected areas. Therefore, by comparing the sum of the projected area obtained from the two sets of meshes, the set of meshes used to calculate the projected areas can be determined. In the case shown in Fig. 7, the front meshes are selected to calculate the projected areas for the intrusion volume.

3.6. *Calculation of aggregate interlock stresses*

The procedure in the previous section is used to calculate the projected areas for an individual intrusion volume. By utilizing the same procedure for all the intrusion volumes of the virtual specimen shown in Fig. 5a, the total projected areas of the crack surface $A_{x,\text{total}}$ and $A_{y,\text{total}}$ can be obtained. Then, the aggregate interlock stresses generated by the crack surface under given kinematics can be calculated by the following equation:

$$\begin{bmatrix} \sigma \\ \tau \end{bmatrix} = \frac{\sigma_{\text{pu}}}{A_{\text{cr,xz}}} \begin{bmatrix} 1 & -\mu \\ \mu & 1 \end{bmatrix} \begin{bmatrix} A_{\text{x,total}} \\ A_{\text{y,total}} \end{bmatrix} \tag{6}$$

where $A_{\text{cr,xz}}$ is the projected area on the x-z plane of the virtual specimen.

It should be mentioned that Eq. (6) is different from Eq. (1). The unit of A_x and A_y in Eq. (1) used in the Two-Phase model is mm^2/mm^2 since the model was derived based on a unit cracked surface, while the unit of $A_{\text{x,total}}$ and $A_{\text{y,total}}$ is mm^2. To convert the results into stresses, the right-hand side must be divided by $A_{\text{cr,xz}}$.

4. Verification against the Two-Phase model

The proposed method can be considered as an extended and generalized version of the Two-Phase model since the assumptions used in the proposed method are the same as those used in the Two-Phase model. The main extension of the proposed method is that it enables the usage

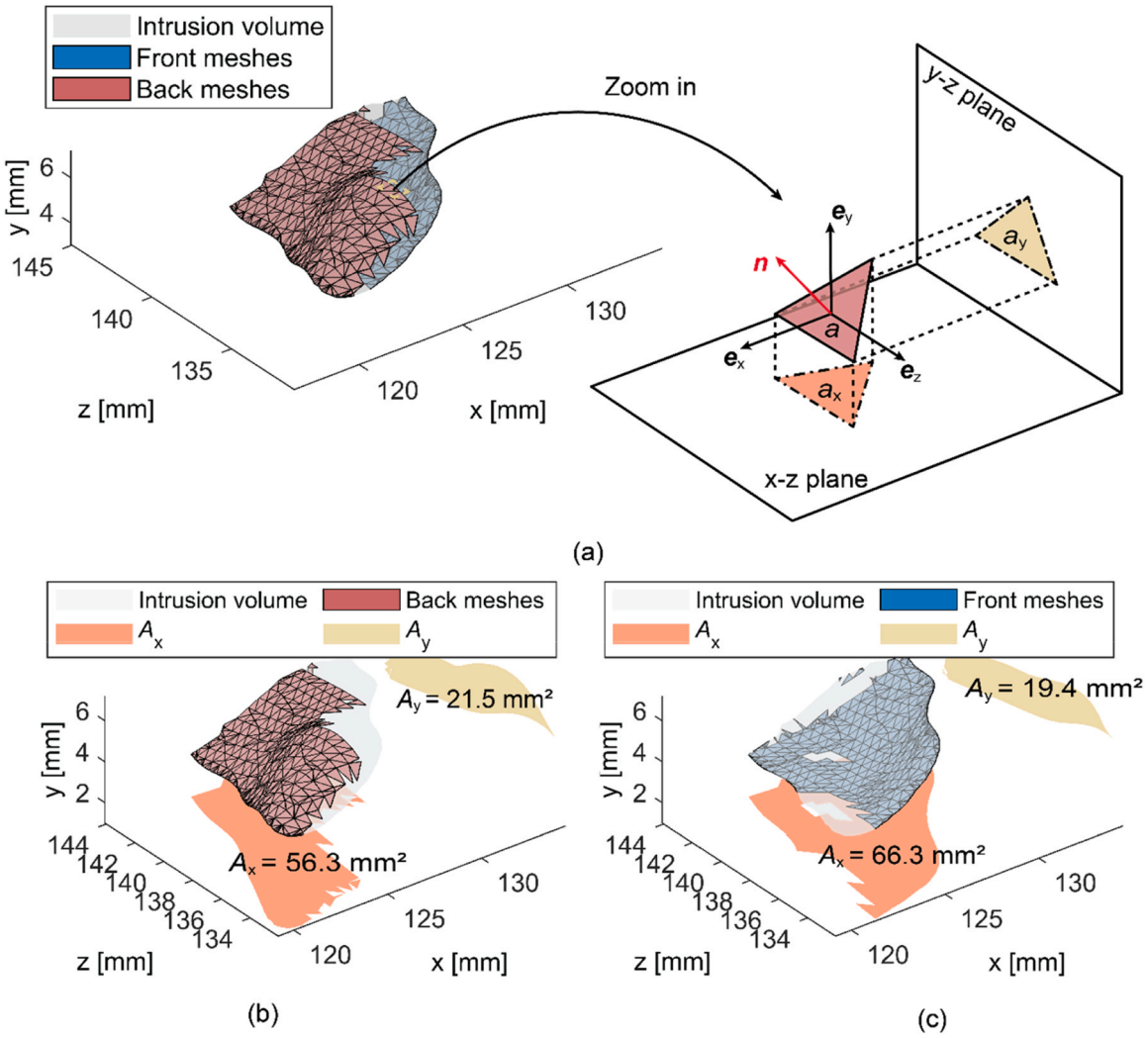

Fig. 7. Calculation of the projected areas: (a) schematic illustration for calculating projected areas; (b) the calculated projected areas based on the back meshes; (c) the calculated projected areas based on the front meshes.

of a real crack surface with random irregularities under the framework of the Two-Phase model. To verify the proposed method, we apply it on a simplified crack surface which strictly follows the same assumptions used in the Two-Phase model. If the proposed method can produce similar predictions as the analytical model, one may conclude that it is equivalent to the analytical model, and this allows for a further investigation of scanned surfaces using the proposed method. The following sections present the detailed procedure of cross-verification against the Two-Phase model.

4.1. Generation of simulated crack surfaces

The simplified crack surface used in the Two-Phase model is a plane crossing several perfectly spherical aggregates. To generate such surfaces, a virtual concrete cube (i.e., 150 mm × 150 mm × 150 mm) filled with perfectly spherical aggregates is first generated. This is achieved by applying the three-dimensional packing algorithm proposed by Al-Jelawy and Al-Rumaithi et al. [37]. The maximum aggregate size D_{max} is set to 32 mm for cube generation. Fig. 8a and b show the generated cube and the corresponding cumulative curve of aggregates. The simulated cumulative curve of aggregates follows the ideal Fuller's distribution.

The particle ratio p_k between aggregate volume and concrete volume used to generate the cube is 0.75 according to the Two-Phase model. It should be noted that the minimum diameter in the simulated cube is set to a quarter of D_{max} to limit the time to randomly assign a spatial location for an aggregate with a small diameter. Accordingly, an adjustment is made in the Two-Phase model when comparing the simulation results with the Two-Phase model. The adjustment is described in the Section 4.2.

In this verification, three cubes are generated. For each cube, nine cross-sections at different heights are selected to create the crack surfaces, leading to 27 surfaces for cross-verification. For the chosen cross-sections, the point cloud data is generated according to the locations of the aggregates. Fig. 8c and d show the point cloud data of two crack surfaces at different heights. The average spacing of the point cloud data is set to around 0.44 mm, comparable to the scanned data used in this paper. With the point cloud data, the proposed method described in Section 3 is used to calculate the aggregate interlock stresses.

In general, the crack surface does not cross the spherical aggregates through their centres, which leads to the aggregates having an embedded depth u, as shown in Fig. 1c. It can be seen that the embedded depth u of the aggregate can affect the calculation of A_x and A_y. In the Two-Phase model, u is assumed to be a random variable evenly distributing within the interval $[0, R]$ to consider the influence of u. In this verification, choosing the cross-sections at different heights of the cubes is considered as an independent random realization of generating different embedded depth u.

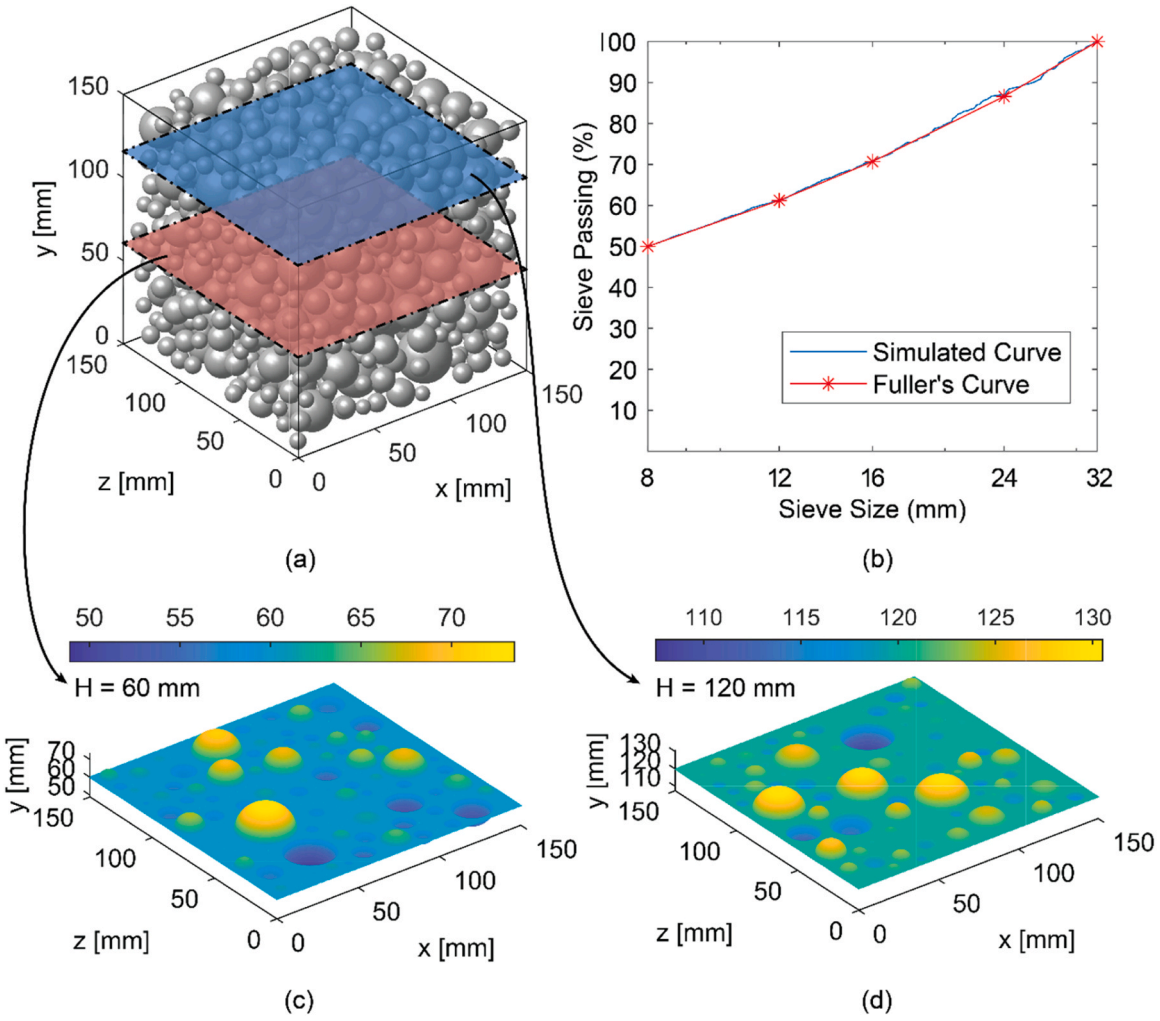

Fig. 8. A simulated cube with maximum aggregate size $D_{max} = 32$ mm and particle ratio $p_k = 0.75$: (a) overview of the simulated cube; (b) comparison between ideal Fuller's distribution and simulated cumulative curve of aggregates; (c) point cloud data of the simulated surface at H = 60 mm; (d) point cloud data of the simulated surface at H = 120 mm.

4.2. Adjustment in the Two-Phase model for verification

As mentioned in Section 4.1, for the sake of computational efficiency, it is chosen to limit the minimum aggregate diameter at $0.25D_{max}$ in the packing algorithm. This limit means that the Two-Phase model has to be modified to neglect the contribution of the aggregates with a diameter smaller than $0.25D_{max}$. This is achieved by adjusting the lower bound D_{min} of the integral equation in the Two-Phase model, as shown in Eq. (7). It should be noted that this adjustment in minimum aggregate size is only used in the verification section due to the limitations of the packing algorithm.

$$\begin{bmatrix} A_y \\ A_x \end{bmatrix} = \int_{D_{min}}^{D_{max}} n(D) \begin{bmatrix} a_{yD} \\ a_{xD} \end{bmatrix} dD \tag{7}$$

$$D_{min} = \max\{0.25D_{max}, f(w,\Delta)\} \tag{8}$$

where a_{xD} and a_{yD} are the expected projected area in the x-z plane and the y-z plane for an aggregate with a diameter D, $n(D)$ is the expected number of intersected aggregates with a diameter of D within a unit length and $f(w,\Delta)$ is a function to determine the D_{min} in the Two-Phase model.

4.3. Verification results and discussions

4.3.1. Overview of used parameters and kinematics

In the verification, a constant initial opening w of 0.5 mm is used, and the sliding Δ_x is applied in the x-direction starting from 0.1 to 4 mm with a step size of 0.2 mm. It should be noted that the chosen kinematics does not affect the generality of the verification. The cube compressive concrete strength $f_{c,cube}$ is assumed to be 57.9 MPa, and the coefficient of friction μ is adopted as 0.4 according to the Two-Phase model.

4.3.2. Verification results and discussions

Fig. 9a and b show the verification regarding the aggregate interlock stresses between the Two-Phase model and the proposed method. Here, the results from the Two-Phase model and the proposed method are referred to as analytical and simulated results respectively. The simulated results are the collection of the results of 27 simulated crack surfaces. The overall tendency of the simulated results is comparable to the analytical results. For a better illustration, the filled colour of the scatter is set with transparency to reflect the concentration level of the results. It can be seen that the simulated results from different crack surfaces are not identical and they are distributed within a certain bandwidth. This distribution reflects the influence of the embedded depth u.

The verification results suggest that the analytical results are on the lower side of the simulated results, especially for the normal stresses.

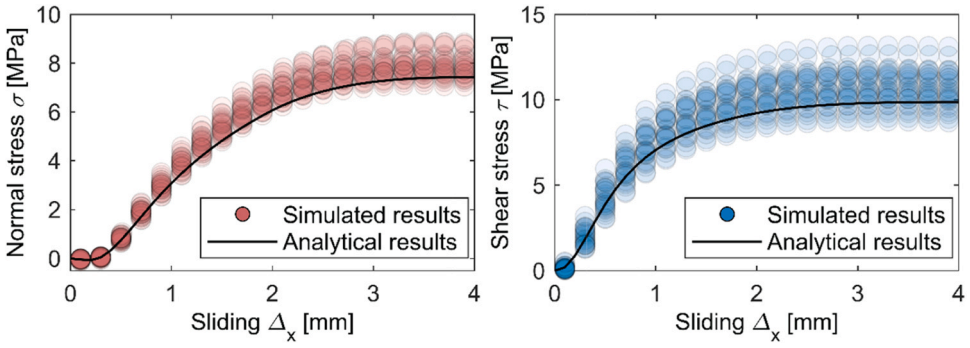

Fig. 9. Verification results between the analytical results and the simulated results: (a) normal stress; (b) shear stress.

One possible reason for this overestimation in the simulated results is that a contact event can also occur between the aggregates in the proposed method. As shown in Fig. 10a, when two aggregates are adjacent and embedded in the opposite crack surfaces respectively, two separate intrusion volumes are considered when the sliding is small. As the sliding increases, these two aggregates start to contact and the two separate intrusion volumes merge into one single intrusion volume, as indicated in Fig. 10b. This merging effect results in larger projected contact areas, especially in the y-direction, compared to the sum of individual projected areas of two small intrusion volumes. Consequently, the calculated interlock stresses are higher than those predicted by the analytical model, which assumes an idealized, independent contact event between aggregate and concrete paste.

On the other hand, the contact event between the aggregates is not considered in the Two-Phase model since it is established based on the contact event between an individual aggregate and cement paste. It is possible to have such contact events between two real crack surfaces. One may argue that the Two-Phase model has indirectly covered this effect through calibration with test data. Therefore, these two contact events are not treated separately in the proposed method. Overall, the performed cross-verification proves the validity of the proposed method and the Two-Phase model.

4.3.3. Sensitivity on crack surface size

The previous section shows that the simulated results based on the crack surface with a size of 150 × 150 mm are scattered. This high scatter could be caused by the crack surface not being large enough to eliminate the influence of embedded depth u. Therefore, the scatter of the simulated results shall be reduced if the crack surface size becomes larger.

In this section, a sensitivity investigation of the influence of crack surface size on the simulated aggregate interlock stresses is conducted. The simulated results of a crack surface size of 150 mm × 150 mm are randomly combined to realize another 27 crack surfaces with a larger size. Fig. 11a and b show the crack surface with sizes of 150 mm × 300 mm and 300 mm × 300 mm after combining two and four smaller surfaces, respectively.

Fig. 11c and d compare the results generated by the surfaces with the sizes of 150 mm × 150 mm and 300 mm × 300 mm. The mean value of collected results from 27 crack surfaces is indicated by a dashed line and the standard deviation is indicated by a band. It can be seen that the mean values from different sizes are very close because the assumptions for aggregate distribution and geometry are the same. However, the standard deviation of the results decreases significantly with a larger crack surface because a larger crack surface can have more varieties for the random variable u, eliminating its influence on the results.

By doing such an analysis, a representative crack surface size can be recommended to determine the aggregate interlock stresses of the actual crack surface. According to the results of the current analysis, it is recommended to use a crack surface with a size of at least 300 mm × 300 mm to determine the aggregate interlock stresses.

5. Application to scanned crack surfaces

5.1. Overview information

In this section, the proposed method is applied to four actual crack surfaces as a demonstration. The four crack surfaces are from splitting tensile tests of four standard concrete cubes. Two of them are made of geopolymer concrete and the other two are made of normal concrete. The 28-day average cube compressive concrete strength of the geopolymer cubes is 57.9 MPa and that of the normal concrete is 58.1 MPa, respectively. The maximum aggregate size of the geopolymer cubes is 16 mm. More information about the mixture design can be found in [30, 38]. The maximum aggregate size of the normal concrete cubes is 32 mm and the mixture composition of normal concrete can be seen in Table 1. The point cloud data is obtained using a handheld scanner HandyScan Black from Creaform [31]. Fig. 12 shows the four scanned surfaces, they are named by Geo-1, Geo-2, Nor-1 and Nor-2. It should be mentioned that only one scanned surface is used for each cube because

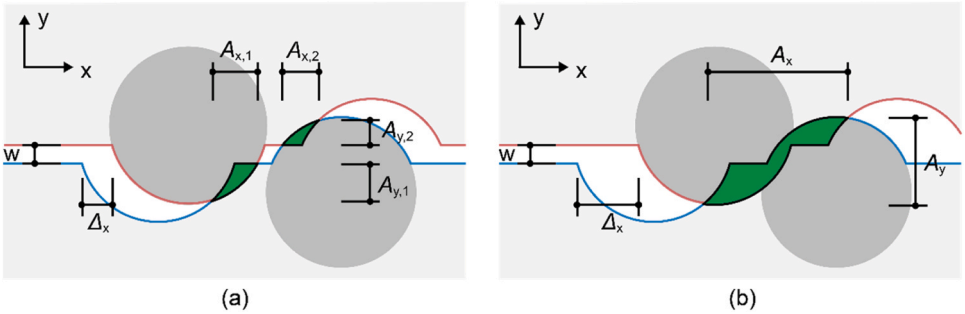

Fig. 10. Contact event between two aggregates: (a) intrusion volumes develop separately when the sliding is relatively small; (b) union of intrusion volumes when the sliding is large.

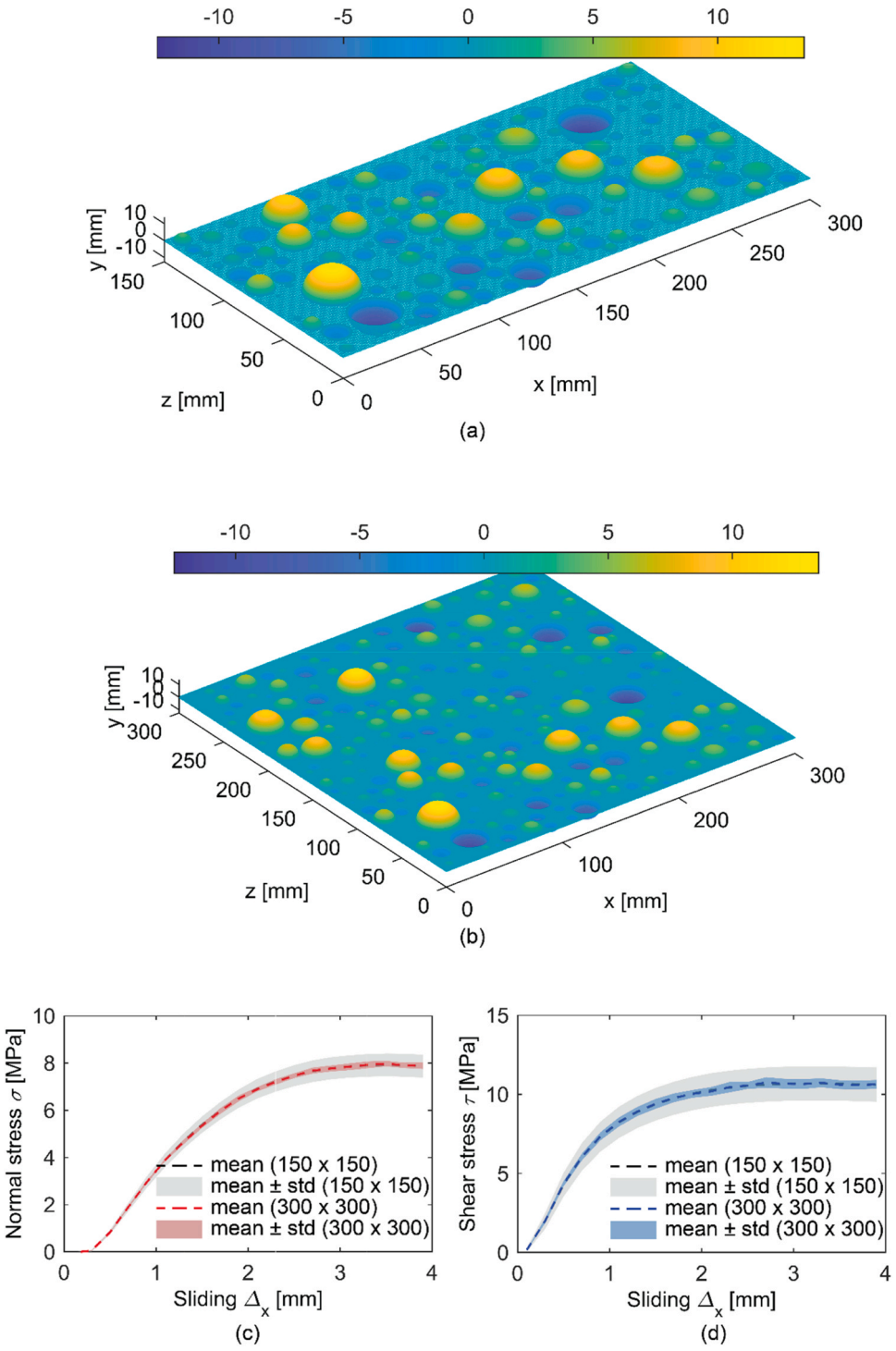

Fig. 11. Sensitivity analysis on the crack surface size: (a) a crack surface with size of 150 mm × 300 mm; (b) a crack surface with size of 300 mm × 300 mm; (c) comparison of statistics from different crack surface sizes in normal stress; (d) comparison of statistics from different crack surface sizes in shear stress;.

Table 1
Mixture composition of normal concrete.

Material	Content [kg/m^3]
CEM IIIB 42.5 N LH/SR	382
Sand 0–4 mm	815
Gravel 4–32 mm	1041
Superplasticizer	1.376
Water	113

the counterpart is assumed to be identical according to the assumption used in the Two-Phase Model.

To quantify the irregularity of a surface, the surface roughness index proposed by Lange et al. [33] is calculated using the following equation:

$$R_s = \frac{A_a}{A_p} \tag{9}$$

where R_s is the surface roughness index, A_a is the actual surface area, A_p is the projected surface area and the projected area in the *x*-*z* plane is

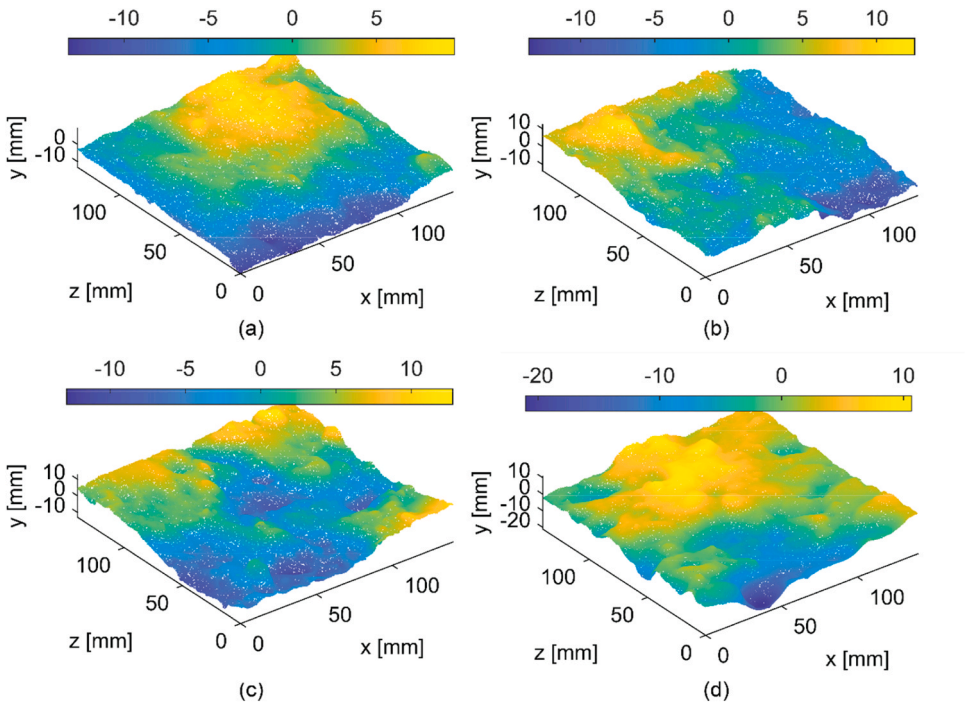

Fig. 12. Scanned crack surfaces: (a) Geo-1; (b) Geo-2; (c) Nor-1; (d) Nor-2.

used in this paper.

As pointed out by Tirassa et al. [21], the surface roughness index can be different if a different point spacing is used. In this calculation, the average spacing of the point cloud is 0.20 mm. Besides the surface roughness index R_s, the conventional morphological metrics to indicate the surface roughness, including the maximum peak height S_p, the maximum valley depth S_v and the maximum surface height S_z, are also calculated.

Table 2 summarizes the mechanical properties and the surface roughness indexes of the scanned cubes. The two types of concrete are in comparable surface roughness index range although their maximum aggregate sizes are different. In both concrete types, the variation of the surface roughness index is large, which is also reported in the work by Tirassa et al. [21].

5.2. Results

In this analysis, the bottom surface is established based on the scanned data and the top surface is assumed to be identical as mentioned above. The deformation described below is only subjected to the top surface, and the bottom surface is assumed to be fixed. The opening is applied in the positive *y*-direction first and the opening is kept constant when a sliding is applied. The sliding is applied in the positive *x*-direction from 0.1 to 4.0 mm with a step size of 0.2 mm to generate one set of results. To investigate the influence of the opening on the aggregate interlock stresses, the opening also varies from 0.1 to 1.1 mm with a step size of 0.2 mm.

Fig. 13a compares the results of the aggregate interlock stresses of Geo-1 and Geo-2 with different crack kinematics. The convention of normal stresses is negative. The solid markers indicate the results of Geo-1, and the hollow markers represent the results of Geo-2. It can be seen that the aggregate interlock stresses generated by Geo-1 and Geo-2 are different. The differences become smaller when the opening is larger. Although the surface roughness index of Geo-1 is smaller, the aggregate interlock stresses generated by Geo-1 are larger than those of Geo-2, especially when the opening is small. This could be caused by the fact that the irregularity of cracked surfaces is not symmetrical, which means that the sliding direction can affect the aggregate interlock responses.

Fig. 13b compares the results of the aggregate interlock stresses of Nor-1 and Nor-2 with different crack kinematics. As expected, under the same kinematics, the aggregate interlock stresses of Nor-1 are larger than those of Nor-2 as the surface roughness index of Nor-1 is higher. The increase in aggregate interlock stresses due to a larger surface roughness index is more significant in the shear stresses. Similar to the observation in Geo1 and Geo-2, the differences in aggregate interlock stresses between two surfaces become smaller as the opening increases.

5.3. Influence of sliding direction

In the demonstration shown in Section 5.2, Geo-2 gives a lower aggregate interlock stresses compared to Geo-1 although the surface roughness index of Geo-2 is higher. One of the possible reasons is that the asperity of the surfaces varies in different directions. For the idealized surfaces shown in Section 4, the asperity is symmetrical since the perfectly spherical aggregates are used and therefore the aggregate interlock responses are the same. While the asperity of the actual crack

Table 2
Mechanical properties and surface roughness indexes of the scanned concrete cubes.

Specimen	Average 28 days cube compressive strength $f_{c,cube}$ [MPa]	Maximum aggregate size D_{max} [mm]	Surface roughness index R_s [-]	Maximum peak height S_p [mm]	Maximum valley depth S_v [mm]	Maximum surface height S_z [mm]
Geo−1	57.9	16	1.115	6.37	6.68	13.05
Geo−2			1.209	7.13	8.86	15.99
Nor−1	58.1	32	1.216	12.74	12.80	25.54
Nor−2			1.147	8.68	14.79	23.48

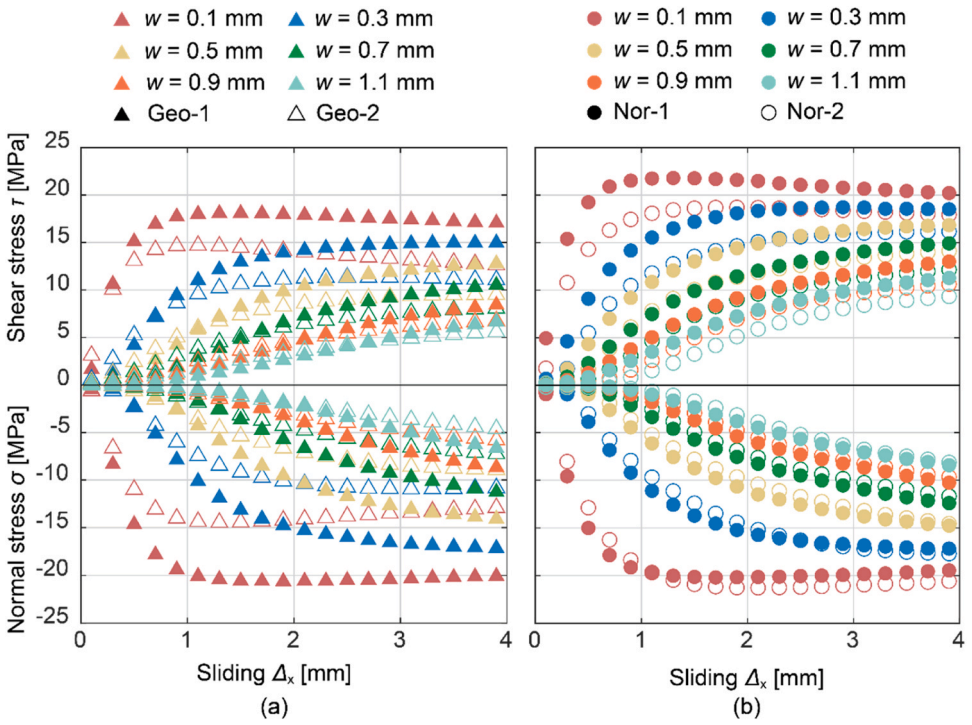

Fig. 13. Aggregate interlock stresses from scanned crack surfaces under different kinematics: (a) results of Geo-1 and Geo-2; (b) results of Nor-1 and Nor-2.

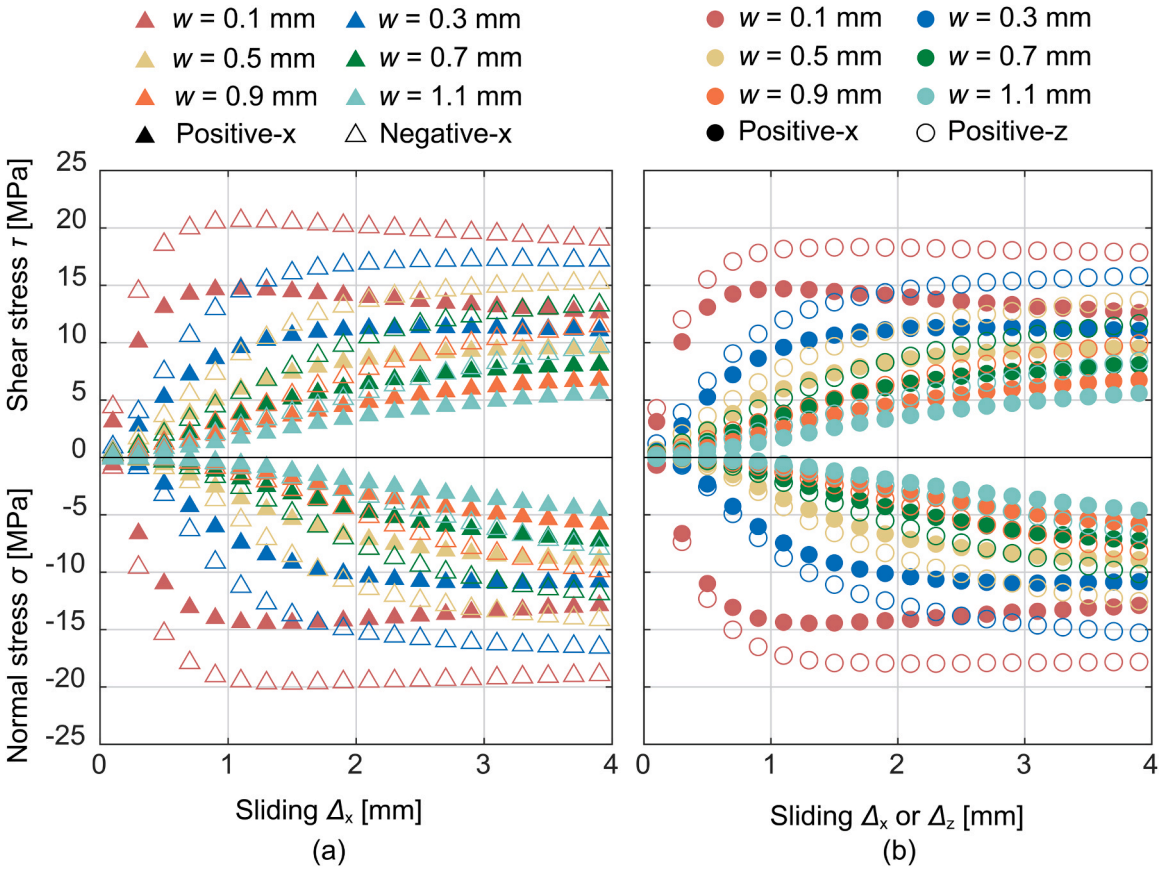

Fig. 14. Influence of sliding direction on aggregate interlock stresses based on Geo-2: (a) comparisons between the positive and negative x-direction; (b) comparisons between the positive x-direction and z-direction.

surfaces is not symmetrical in most cases, therefore, applying the sliding in different directions may result in different aggregate interlock stresses.

In this section, two additional analyses with the sliding in the negative *x*-direction and the positive *z*-direction are conducted using Geo-2 to compare against the previous calculation, i.e., the sliding in the positive *x*-direction. Fig. 14 compares the results of Geo-2 under different sliding directions. It can be seen that the sliding directions can significantly affect the aggregate interlock stresses.

The variation of aggregate interlock responses in different directions can be explained using the distribution of outward unit normal vectors $\boldsymbol{n}$. Fig. 15 shows an arbitrary crack surface under pure sliding in the positive *x*-direction subjected to the top surface. The directional vector of the sliding $\boldsymbol{s}$ can be considered to be (1,0). It can be seen that for the bottom surface only the locations, which satisfy the condition $\cos(\boldsymbol{n},\boldsymbol{s}) \leq 0$, as highlighted by green in Fig. 15, have the potential to contribute to the intrusion volume. By calculating the projected area A_y of those locations, a possible maximum contact area $A_{y,max}$ can be obtained.

Table 3 summarizes the results of $A_{y,max}$ in four different directions. The results show that there are differences in $A_{y,max}$ in different directions and these differences in $A_{y,max}$ align with the variation in aggregate interlock stresses. Based on the results, It can be expected that the aggregate interlock stresses in the negative *z*-direction are the smallest among the four directions. The deviations of $A_{y,max}$ observed in different directions may be attributed to the spatial variation of concrete paste strength and the randomness of the fracture process.

This study shows that other than the surface roughness index, other parameters such as the sliding direction can affect the aggregate interlock stresses. To determine more representative aggregate interlock contributions, the average or characteristic value of the results from different directions should be considered. Besides, a sample with a larger size is needed as presented in Section 4.3.3.

5.4. Comparison against theoretical models

As mentioned in the introduction, there are several theoretical models of aggregate interlock in literature. In this section, three mechanical models for aggregate interlock including the Two-Phase model [1,29], the Contact Density Model [2,3] and the Rough Crack Model [4] are used to calculate the aggregate interlock stresses and to make a comparison against the results obtained from the four scanned surfaces.

In the comparison, three crack openings are selected: 0.1 mm, 0.5 mm and 1.1 mm. Although using a crack surface with a small size could result in a high scatter, it is still beneficial to compare the tendency. Fig. 16a compares the results from scanned surfaces of geopolymer concrete and the calculations based on theoretical models. The results of the scanned surfaces are obtained based on the sliding in the positive *x*-direction. The scanned results are aligned with the results given by the Two-Phase model although the aggregate interlock stresses of Geo-2 are lower due to the sliding direction. The Contact Density Model gives higher values than the scanned results in general except when the opening is small. Regarding the results given by the Rough Crack Model, they are only aligned with the scanned results when the opening and sliding are large.

Although the results from the Two-Phase model and scanned surface

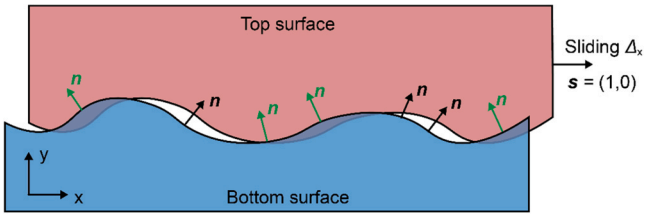

Fig. 15. Schematic illustration of an arbitrary cracked surface.

Table 3
Possible maximum projected area $A_{y,max}$ of Geo-2 in different directions.

Direction	Sliding vector $\boldsymbol{s}$	Possible maximum projected area $A_{y,max}$ [mm^2]
Positive *x*-direction	(1,0,0)	3069.5
Negative *x*-direction	(−1,0,0)	4048.8
Positive *z*-direction	(0,1,0)	3655.0
Negative *z*-direction	(0,−1,0)	2416.3

are generally aligned, there are some deviations when the sliding is smaller. This can be attributed to the recycled aggregates in the used geopolymer cubes. The recycled aggregates have a lower strength due to the thermal processing and the breakage of the aggregates can be observed on the crack surface [30] after the splitting tensile test, leading to reduced aggregate interlock stresses.

It is worthwhile to point out that the Contact Density Model is closer to the scanned results in both normal and shear stresses when the opening is 0.1 mm. However, as the opening increases, the Contact Density Model produces much higher results. This could be because the aggregate interlock stresses are strongly related to the crack surface geometry when the crack opening is small. The crack surface geometry is well captured by the crack plane angle distribution by the Contact Density Model, which is also demonstrated in [21,27]. As the opening increases, the distribution of larger aggregates plays a more important role since the aggregate interlock stresses are mainly contributed by the contact between several aggregates and the cement paste. The Contact Density Model does not account for aggregate distribution, while the Two-Phase model does. This explains why the scanned results align more with the Two-Phase model when the opening is larger.

Fig. 16b compares the results from scanned surfaces of normal concrete and the calculations based on theoretical models. The results of the scanned surfaces are obtained based on the sliding in the positive *x*-direction. Similar conclusions can be drawn as previously. However, since the normal concrete is used and the aggregates are intact on the crack surface, it can be seen that the results given by the Two-Phase model are comparable in magnitude compared to the scanned results even when the sliding is small.

5.5. Discussions on the surface roughness index

As shown in Sections 5.2 and 5.3, despite the influence of the sliding, the aggregate interlock stresses can be similar even when the surface roughness indexes are different. This mismatch may imply that the surface roughness index cannot sufficiently reflect the influence of surface irregularity on aggregate interlock stresses. This mismatch between the surface roughness index and the aggregate interlock stresses can be exemplified by using an extreme example shown in Fig. 17a and b. The first surface is a square with a hemisphere with a radius of 12 mm in the centre and the second is a square with a half cube with a side length of 15 mm. The surface roughness indexes of these two surfaces are the same according to Eq. (9), which are 1.181. Moreover, the two surfaces are symmetrical, so the sliding direction does not affect the projected area calculation.

Applying an opening of 0.5 mm and sliding in the positive x-direction, the projected area in two directions can be obtained, and the results are summarized in Fig. 17c and d. It can be seen that the projected area developments of the two surfaces are very different, although the surface roughness indexes are the same. The surface with a sphere has a larger projected area when the sliding is larger compared to the one with a cube. This can be explained by the concept of the possible maximum projected area $A_{y,max}$ mentioned in Section 5.3. For the sphere surface, the $A_{y,max}$ is 226.3 mm^2, while that of the cube surface is 112.5 mm^2.

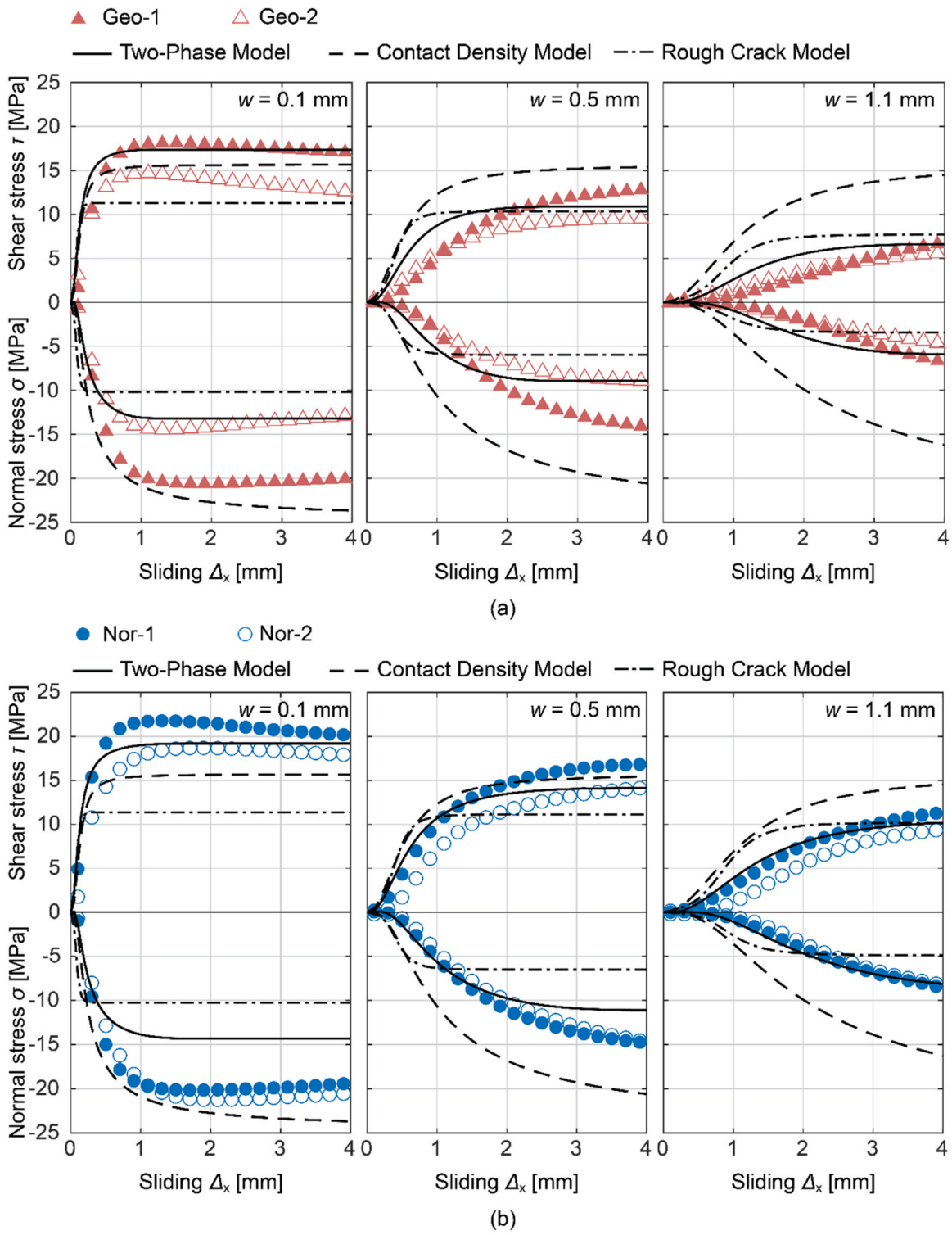

Fig. 16. Comparison between the scanned results and the calculations based on different theoretical models: (a) results of Geo-1 and Geo-2; (b) results of Nor-1 and Nor-2.

5.6. Limitations and possible applications

The demonstrations shown in Section 5 show the feasibility of the proposed methodology in actual crack surfaces and the comparisons against the theoretical models are promising, especially against the Two-Phase Model. However, it should be noted that the comparisons conducted in this paper are qualitative because there is a lack of experimental validation of the proposed method. For future studies, it is recommended to perform 3D scanning before and after the push-off test, then use the proposed method to calculate the aggregate interlock stresses and compare them to the experimental results. On the other hand, numerical validations based on continuum and discrete mechanics are also recommended to further validate the proposed method, which can be an essential complement to experimental approaches.

If the proposed method can be experimentally or numerically validated, it can be considered as an extension of the Two-Phase Model. The

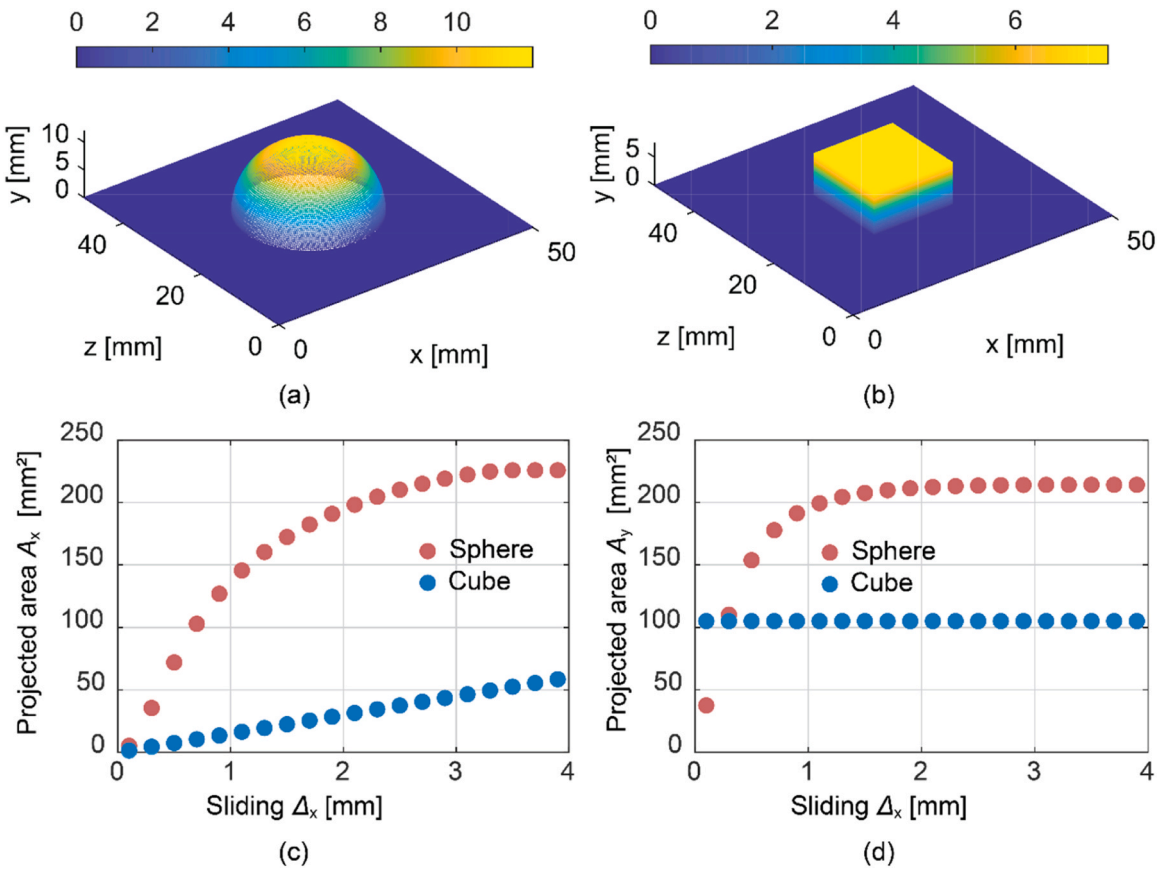

Fig. 17. Illustration of the influence of the surface roughness index: (a) artificial surface with a hemisphere; (b) artificial surface with a half cube; (c) development of the projected area A_x between two surfaces; (d) development of the projected area A_y between two surfaces.

proposed method can be used as a powerful tool to further investigate the aggregate interlock stresses for different types of new concrete. For engineering practice, the aggregate interlock stresses of new types of concrete can be determined by scanning several sample crack surfaces, which is beneficial for design and assessment.

Regarding future research, a more extensive and quantitative study of the influence of the surface roughness on the aggregate interlock stresses, where the selection of the roughness parameter must also be taken into account, can be conducted. Moreover, for concrete types in which a significant portion of aggregates are expected to break, the assumption concerning contact pressure between the cement matrix and the aggregates may not be valid and thus requires experimentally recalibration. Besides, recent experimental research by Autrup et al. [39] and numerical research by Ungermann et al. [40] on aggregate interlock modelling have indicated that the aggregate interlock mechanism exhibits a kinematics dependency and the original Two-Phase model overestimates the aggregate interlock stresses under the mixed mode loading. This overestimation may be attributed to the fact that the contact pressure is not constant. Moreover, as pointed out by Ulaga [41], the strength of concrete paste can vary spatially, which may influence the aggregate interlock responses and should be addressed in future research. The proposed method can be considered a tool to conduct such an investigation and can lead to better modelling of the aggregate interlock.

6. Conclusions

The present paper proposes a generalised method to determine the aggregate interlock contribution of different types of concrete using real crack surfaces from 3D scanning. The aggregate interlock stresses are calculated based on assumptions proposed by the Two-Phase model. The proposed method is cross-verified against the Two-Phase model using idealized crack surfaces with spheres. Then, the proposed method is further implemented in four scanned crack surfaces from cubes after splitting tensile tests to prove its feasibility. The influence of the surface roughness index on the aggregate interlock stresses is discussed using the proposed method. The proposed method shows great potential for further refined investigation of aggregate interlock in future studies. The results and discussion lead to the following conclusions as follows.

Regarding the cross-verification:

- The cross-verification based on the idealized surfaces proves that the proposed method is equivalent to the original Two-Phase model and the proposed method can be used as the extended Two-Phase model.
- In the cross-verification, the analytical calculation from the Two-Phase model is the lower bound of the simulated results given by the proposed method, since the contact event between the aggregates is considered in the proposed method.

Regarding the application to scanned surfaces:

- The application to actual crack surfaces proves the feasibility of the proposed method.
- According to the aggregate interlock responses given by the proposed method, the surface roughness index may not sufficiently reflect its impact on the aggregate interlock responses.
- Moreover, the sliding direction can significantly affect the aggregate interlock responses. To determine representative aggregate interlock responses, it is suggested to use the average or characteristic value of the results obtained from different sliding directions.

The current study aims to propose a framework to apply the Two-

Phase Model, which has been implemented and recognised in practice for many years, to more general crack surfaces with the consideration of the actual irregularity of the concrete mesoscale structure. Nevertheless, the current methodology has only been verified against the analytical model and applied to several scanned crack surfaces. Although the preliminary results show that the proposed method can reflect the influence of irregularity of crack surfaces on aggregate interlock stresses, it is important to note that further experimental or numerical validations are highly encouraged in future work.

CRediT authorship contribution statement

Jiandong Lu: Writing – original draft, Visualization, Validation, Resources, Methodology, Investigation, Formal analysis, Data curation, Conceptualization. **Max A.N. Hendriks:** Writing – review & editing, Supervision, Resources, Project administration, Methodology, Conceptualization. **Joost Walraven:** Writing – review & editing, Supervision, Methodology. **Yuguang Yang:** Writing – review & editing, Supervision, Resources, Project administration, Methodology, Funding acquisition, Conceptualization.

Declaration of Competing Interest

The authors declare that they have no known competing financial interests or personal relationships that could have appeared to influence the work reported in this paper.

Acknowledgement

The author Jiandong Lu would like to acknowledge the funding support from China Scholarship Council (CSC) under the grant CSC No. 202106150029.

Data Availability

Data will be made available on request.

References

[1] Walraven JC. Fundamental analysis of aggregate interlock. J Struct Div 1981;107:2245–70.
[2] Li B, Maekawa K, Okamura H. Contact density model for cracks in concrete. IABSE Colloq Delft 1987:51–62.
[3] Li B. Contact density model for stress transfer across cracks in concrete. J Fac Eng 1989:9–52.
[4] Bažant ZP, Gambarova P. Rough cracks in reinforced concrete. J Struct Div 1980;106:819–42.
[5] Vecchio FJ, Collins MP. The modified compression-field theory for reinforced concrete elements subjected to shear. Acids J 1986;83:219–31.
[6] Muttoni A, Fernández Ruiz M. Shear strength of members without transverse reinforcement as function of critical shear crack width. Acids Struct J 2008;105:163–72.
[7] Cavagnis F, Fernández Ruiz M, Muttoni A. A mechanical model for failures in shear of members without transverse reinforcement based on development of a critical shear crack. Eng Struct 2018;157:300–15.
[8] Yang Y, Walraven J, Uijl Jd. Shear behavior of reinforced concrete beams without transverse reinforcement based on critical shear displacement. J Struct Eng 2017;143:04016146.
[9] Yang Y. Shear Behaviour of Reinforced Concrete Members without Shear Reinforcement [PhD thesis]; 2014.
[10] Classen M. Shear Crack Propagation Theory (SCPT)–the mechanical solution to the riddle of shear in RC members without shear reinforcement. Eng Struct 2020;210:110207.
[11] Marí A, Bairán J, Cladera A, Oller E, Ribas C. Shear-flexural strength mechanical model for the design and assessment of reinforced concrete beams. Struct Infrastruct Eng 2014;11:1399–419.
[12] Cladera A, Marí A, Bairán JM, Ribas C, Oller E, Duarte N. The compression chord capacity model for the shear design and assessment of reinforced and prestressed concrete beams. Struct Concr 2016;17:1017–32.
[13] Cladera A, Marí A, Ribas C, Bairán J, Oller E. Predicting the shear–flexural strength of slender reinforced concrete T and I shaped beams. Eng Struct 2015;101:386–98.
[14] Fédération Internationale du Béton (fib). fib Model Code for Concrete Structures 2010. Ernst & Sohn; 2013. p. 434.
[15] CEN/TC250/SC2/WG1. "Coordination and Editorial Panel". Eurocode 2: Design of concrete structures - Part 1-1: General rules - Rules for buildings, bridges and civil engineering structures. prEN 1992-1-1:2021-09. Brussels, Belgium: Comité Européen de Normalisation 2021, p. 377.
[16] Walraven JC, Stroband J. The behaviour of cracks in plain and reinforced concrete subjected to shear. IABSE Colloq Adv Mech Reinf Concr Final Rep 1981:227–52.
[17] Bentz EC. Sectional analysis of reinforced concrete members. Toronto: University of Toronto; 2000.
[18] Perera S, Mutsuyoshi H. Shear behavior of reinforced high-strength concrete beams. Acids Struct J 2013;110.
[19] Fédération Internationale du Béton (fib). fib Model Code for Concrete Structures 2020. Ernst & Sohn; 2024. p. 434.
[20] Yang Y, den Uijl J, Walraven J. Critical shear displacement theory: on the way to extending the scope of shear design and assessment for members without shear reinforcement. Struct Concr 2016;17:790–8.
[21] Tirassa M, Fernández Ruiz M, Muttoni A. Influence of cracking and rough surface properties on the transfer of forces in cracked concrete. Eng Struct 2020;225.
[22] Zhou G, Xu Z. 3D mesoscale investigation on the compressive fracture of concrete with different aggregate shapes and interface transition zones. Constr Build Mater 2023;393:132111.
[23] Eliáš J, Stang H. Lattice modeling of aggregate interlocking in concrete. Int J Fract 2012;175:1–11.
[24] Jayasinghe T, Gunawardena T, Mendis P. Aggregate interlock in fractured concrete mesoscale models: a novel finite element modelling approach. Arch Civ Mech Eng 2022;22:165.
[25] Wang P, Gao N, Ji K, Stewart L, Arson C. DEM analysis on the role of aggregates on concrete strength. Comput Geotech 2020;119:103290.
[26] Bolander JE, Eliáš J, Cusatis G, Nagai K. Discrete mechanical models of concrete fracture. Eng Fract Mech 2021;257:108030.
[27] Presvyri S, Yang Y, Hendriks M, Visser J, Hordijk D. On the extension of walraven's aggregate interlock model based on laser scanned crack surface. Proc Fib Symp 2019:937–44.
[28] Fuller WB, Thompson SE. The laws of proportioning concrete. Trans Am Soc Civ Eng 1907;59:67–143.
[29] Walraven J.C. Aggregate interlock: a theoretical and experimental analysis. 1980.
[30] Lu J, Yang Y, van der Ham H, Fu D. Structural Behaviour of Slender Geopolymer Concrete Beams Without Stirrups. International Symposium of the International Federation for Structural Concrete. Springer; 2023. p. 835–45.
[31] Creaform 3d. The 3D-Scanner HandySCAN 3D. 2020.
[32] Huber T, Huber P, Kollegger J. Influence of aggregate interlock on the shear resistance of reinforced concrete beams without stirrups. Eng Struct 2019;186:26–42.
[33] Lange DA, Jennings HM, Shah SP. Relationship between fracture surface roughness and fracture behavior of cement paste and mortar. J Am Ceram Soc 1993;76:589–97.
[34] Di Angelo L, Di Stefano P, Giaccari L. A new mesh-growing algorithm for fast surface reconstruction. ComputAided Des 2011;43:639–50.
[35] Tran AP, Yan S, Fang Q. Improving model-based functional near-infrared spectroscopy analysis using mesh-based anatomical and light-transport models. Neurophotonics 2020;7:015008.
[36] Fang Q, Boas DA. Tetrahedral mesh generation from volumetric binary and grayscale images. 2009 IEEE International Symposium on Biomedical Imaging: From Nano to Macro. Ieee; 2009. p. 1142–5.
[37] Al-Jelawy HM, Al-Rumaithi A, Fadhil AT, Naji AJ. Mesoscale modeling of fracture in cement and asphalt concrete. PrzegląD Nauk żynieria i Kształtowanie Środowiska 2021;30.
[38] van der Ham H, Janssen T. Prestressed geopolymer concrete bridge with 100% secondary aggregates. 6th fib International Congress on Concrete Innovation for Sustainability, 2022: fib. The International Federation for Structural Concrete; 2022. p. 2419–28.
[39] Autrup F, Jørgensen HB, Hoang LC. The influence of small amounts of shear reinforcement on the shear-transferring mechanisms in RC beams: an analysis based on refined experimental measurements. Struct Concr 2022.
[40] Ungermann J, Adam V, Classen M. Fictitious rough crack model (FRCM): a smeared crack modelling approach to account for aggregate interlock and mixed mode fracture of plain concrete. Materials 2020;13:2774.
[41] Ulaga T. Betonbauteile mit stab-und lamellenbewehrung: verbund-und zuggliedmodellierung: vdf Hochschulverlag AG; 2003.